AIAA JOURNAL
Vol. 30, No. 10, October 1992

# Numerical Simulation of Slot Injection into a Turbulent Supersonic Stream

Donald P. Rizzetta*
*Wright Laboratory, Wright-Patterson Air Force Base, Ohio 45433*

**Steady flowfields resulting from slot injection at the surface of a flat plate in a freestream with a Mach number of 3.7 and a unit Reynolds number of $5.83 \times 10^6$/m were simulated numerically by integration of the time-dependent compressible mass-averaged Navier-Stokes equations. Effects of fine scale turbulence were represented by a two-equation ($k$-$\epsilon$) closure model that included a generalized formulation, low Reynolds number terms, and a compressibility correction. A grid mesh step-size study is provided to assess resolution requirements of the numerical solutions, and the effect of the compressibility correction is examined. A total of 15 cases were computed, comprising a range of slot widths and slot total pressure ratios. Comparison is made with experimental data in terms of surface static pressure distributions, the length of the upstream separation region, and the height of the Mach surface.**

## Nomenclature

$C_f$ = skin friction coefficient, $(\mu \partial u/\partial n)_w / \frac{1}{2}\rho_\infty u_\infty^2$
$F, G$ = vector fluxes
$H$ = vector source term
$h$ = height of Mach surface
$k$ = turbulence kinetic energy
$l$ = length from plate leading edge to slot centerline
$M_\infty$ = freestream Mach number
$M_t$ = local turbulence Mach number, $(k/\gamma RT)^{1/2}$
$n$ = direction normal to plate surface
$P_j$ = total pressure of jet
$P_0$ = total pressure of freestream
$p$ = static pressure
$R$ = gas constant
$Re$ = unit Reynolds number based on freestream conditions
$T$ = static temperature
$T_i$ = freestream turbulence intensity, $[(2/3)k_\infty]^{1/2}/u_\infty$
$t$ = time
$U$ = vector of dependent variables
$u, v$ = Cartesian velocity components in $x, y$ directions
$w$ = slot width
$x, y$ = Cartesian coordinates in streamwise and normal directions
$x_{sep}$ = separation length
$y^+$ = law-of-the-wall coordinate, $[(\rho/\mu)(\partial u/\partial y)]_w^{1/2} y$
$\alpha$ = compressibility correction coefficient, 1.0
$\gamma$ = specific heat ratio, 1.4 for air
$\Delta x, \Delta y$ = computational mesh step sizes
$\epsilon$ = turbulence energy dissipation
$\mu, \mu_t$ = molecular and turbulent viscosity coefficients
$\xi, \eta$ = computational coordinates in streamwise and normal directions
$\xi_x, \xi_y, \eta_x, \eta_y$ = metric coefficients of the coordinate transformation
$\rho$ = fluid density

*Subscripts*

$t$ = turbulent
slot = evaluated at nozzle exit
$w$ = wall value
$\infty$ = freestream value

*Superscript*

$*$ = sonic condition

## Introduction

THE flowfield resulting from the injection of secondary fluid normal to the turbulent boundary layer over a flat plate in an external supersonic stream is of both fundamental and practical interest. Such flows may be encountered in thrust vector regulation systems of rocket motors, in reaction control jets of high-speed flight vehicles, and in the injection of gaseous fuel or for mixing enhancement in supersonic combustors. A number of experimental investigations[1-9] have been conducted to describe the characteristics of these flowfields, whose general features are now well understood.

The configuration to be considered is depicted in Fig. 1 and consists of the supersonic flow over a flat plate with a sharp leading edge that is located a distance $l$ upstream of the centerline of a converging slot nozzle of width $w$. Injection occurs normal to the freestream, and it is assumed that the jet is underexpanded such that sonic conditions prevail across the nozzle exit in the plane of the plate surface. Expansion of the jet rapidly occurs as it leaves the nozzle and penetrates the otherwise undisturbed turbulent boundary layer, developing a complex inviscid/viscous interaction that is represented sche-

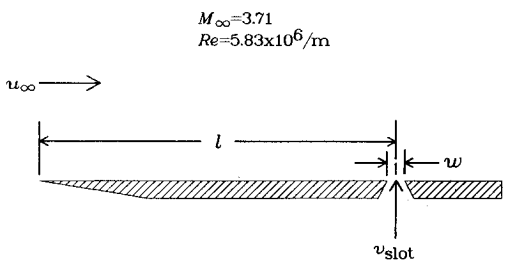


**Fig. 1 Slot injection geometry.**

Received Oct. 21, 1991; presented as Paper 92-0827 at the AIAA 30th Aerospace Sciences Meeting, Reno, NV, Jan. 6-9, 1992; revision received Feb. 27, 1992; accepted for publication March 2, 1992. 

*Aerospace Engineer, Aeromechanics Division, Flight Dynamics Directorate. Associate Fellow AIAA.

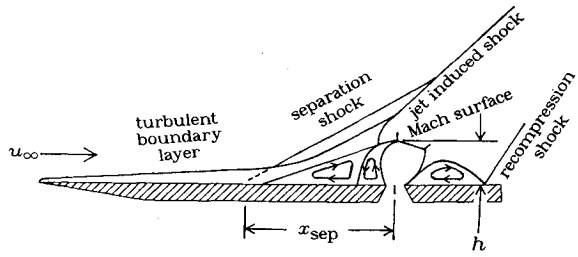


**Fig. 2 Schematic representation of slot injection flowfield.**

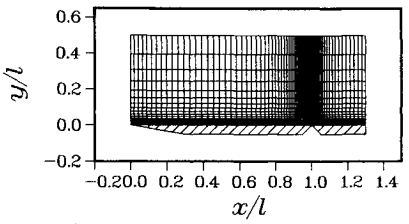


**Fig. 3 Coarse mesh computational grid.**

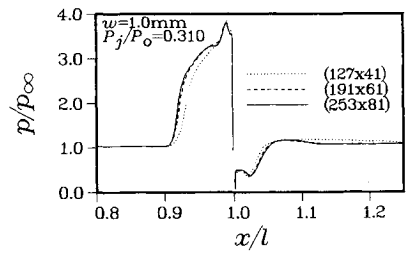


**Fig. 4 Effect of grid refinement on surface static pressure distribution for $w$ = 1.0 mm and $P_j/P_0$ = 0.310.**

matically by Fig. 2. In the inviscid portion of the flowfield, an induced shock wave is generated due to blockage of the freestream, and is often referred to as the bow shock. Upstream of the jet, the induced shock provokes separation of the boundary layer, creating two contiguous regions with fluid recirculating in opposite directions. A shock wave forms upstream of this separation due to viscous displacement and can intersect the jet-induced shock. Upon exiting the nozzle, expansion of the jet flow is followed by deceleration that produces a normal shock to attain pressure equilibrium, giving rise to a Mach surface commonly designated the Mach disk for circular jets. Downstream of the jet, the main flow is eventually directed parallel to the plate, resulting in a recompression shock and a corresponding separated flow region.

This physical situation has often been compared with that of the flow over a protuberance mounted on a flat plate,[1] which produces a similar displacement effect but differs in structure. Specifically, neither the Mach surface nor the second upstream recirculating flow region are present.

A number of numerical calculations have been performed to simulate jet interaction flowfields. Among these, the computations of Shang et al.[10] considered a circular jet issuing from a body of revolution at angle of attack in hypersonic flow, whereas those of Rhie and Syed[11] described the three-dimensional flow through a nonreacting supersonic combustor with injection. Thompson[12] numerically duplicated the test conditions of Spaid and Zukoski,[7] employing an algebraic eddy viscosity model. Just one case was calculated, and agreement between the computed surface pressure distribution and experimental data was poor, due to the inability of the computation to adequately predict the length of the recirculating flow regions. Computations for circular jets were performed by Lytle et al.[13] using a composite algebraic turbulence closure model and an adaptive grid.

The present investigation attempts to numerically reproduce the slot injection experiments of Aso et al.[9] at a freestream Mach number of 3.7 and a unit Reynolds number of $5.83 \times 10^6$/m. These results were selected because they represent a comprehensive set of data for three different slot widths ($w$ = 0.5, 1.0, and 2.0 mm) and a range of slot total pressure ratios ($0.1 \le P_j/P_0 \le 0.5$). In addition to surface static pressure distributions, the experimentally determined length of the upstream separation region $x_{sep}$ and the height of the Mach surface $h$ are available for comparison.

Effects of fine scale turbulence are simulated by an eddy viscosity model that is specified as a function of the turbulence kinetic energy $k$ and the turbulence energy dissipation $\epsilon$. For this purpose, the generalized compressible formulation due to Gerolymos[14] is used, which incorporates low Reynolds number terms to model near-wall effects. The compressibility correction proposed by Sarkar et al.[15] has also been employed. Because this set of equations requires no predefined turbulence length scales or wall functions, either solid surfaces or the jet exit plane may be treated by a mere change of boundary conditions. Although length scales of algebraic closure models are readily prescribed for simple unseparated flows, their implementation for complex configurations may be tedious. Moreover, no rational modification for simulating jet injection is apparent. Thus the present formulation is attractive for the description of intricate fluid structures, as well as for the computation of flows about elaborate geometric shapes.

It is the purpose of this study to numerically duplicate the extensive set of data provided by experiment so that the adequacy of the turbulence modeling may be assessed with regard to nozzle width and slot pressure ratio for jet injection flowfields. A grid mesh step-size study is provided to address the issue of resolution requirements of the solutions, and the effect of the compressibility correction is examined.

## Governing Equations

The governing equations were taken to be the unsteady compressible two-dimensional Navier-Stokes equations written in mass-averaged variables and expressed notationally in the following flux-vector chain-rule conservative form:

$$\frac{\partial U}{\partial t} + \xi_x \frac{\partial F}{\partial \xi} + \xi_y \frac{\partial G}{\partial \xi} + \eta_x \frac{\partial F}{\partial \eta} + \eta_y \frac{\partial G}{\partial \eta} + H = 0 \qquad (1)$$

Effects of fine scale turbulence are accounted for by specifying a turbulent Prandtl number of 0.90 and by incorporating a two-equation closure model for the turbulence kinetic energy $k$ and the turbulence dissipation $\epsilon$. This set of equations was originally devised by Jones and Launder[16] for the computation of incompressible boundary-layer flows. To improve near-wall modeling, low Reynolds number terms were subsequently appended to the equations by Launder and Sharma,[17] whose formulation was considered to perform well in the comprehensive comparative study by Patel et al.[18] The choice of this model was motivated by the fact that the Cartesian-tensor form of the equations is directly extendable to three spatial dimensions and does not require knowledge of the distance from solid boundaries. Furthermore, because the equation for $\epsilon$ is formulated in terms of the difference between the dissipation of the turbulent kinetic energy and the dissipation of homogeneous turbulence, homogeneous boundary conditions for both $k$ and $\epsilon$ may be applied at solid surfaces, thereby facilitating the computation of flows about complex configurations.

The correction proposed by Sarkar et al.[15] has also been adopted to more adequately represent compressible flows. This term accounts for the effect of Mach-number-induced changes in turbulent structure due to energy dissipation. It has been shown to be important for the computation of compressible mixing layers[15,19] and, because it arises as a consequence of dilatation, has been referred to as "dilatation dissipation" by Zeman.[19]

Apart from the compressibility correction, the governing equations are identical to those employed by Gerolymos[14] for the simulation of several transonic channel flowfields and may be found in their entirety in Ref. 20. Sutherland's law for the molecular viscosity coefficient and the perfect gas relationship were employed together with Stokes hypothesis. The compressibility correction appears only in the source term for the turbulent kinetic energy equation and is specified as the function of the local turbulence Mach number $\alpha\rho\epsilon M_t^2$, with $\alpha = 1.0$ as suggested by Sarkar et al.[15]

Because the freestream is supersonic, the upstream computational boundary was located just ahead of the sharp leading edge of the flat plate where all dependent variables were assigned their respective freestream values. For this purpose, a turbulence intensity level $T_i$, defined as

$$T_i = (\tfrac{2}{3}k_\infty)^{1/2}/u_\infty \tag{2}$$

was assumed in the freestream to prescribe the magnitude of the turbulence kinetic energy. In all of the results presented here, this level was taken as $T_i = 0.005$. Corresponding values of the freestream dissipation were then determined by requiring that $\mu_{t_\infty} \approx \mu_\infty$. Although the turbulent equations are somewhat sensitive to the freestream levels of $k$ and $\epsilon$, preliminary flat plate computations at the given flow conditions indicated that the aforementioned choices resulted in a boundary layer that was essentially fully turbulent near the leading edge.

The upper boundary of the computational domain was chosen sufficiently far from the plate such that shock waves generated in the interior passed out of the flowfield at the downstream boundary. Accordingly, freestream conditions prevailed for all dependent variables at the top of the domain. Downstream, a simple first-order extrapolation from the interior was applied, corresponding to the condition

$$\frac{\partial U}{\partial \xi} = 0 \tag{3}$$

On solid surfaces, the no-slip conditions

$$u = v = 0 \tag{4}$$

were invoked, along with

$$\frac{\partial p}{\partial n} = 0 \tag{5}$$

and the adiabatic wall condition

$$\frac{\partial T}{\partial n} = 0 \tag{6}$$

Because of the inclusion of the low Reynolds number terms in the $k$-$\epsilon$ equations, the homogeneous conditions

$$k = \epsilon = 0 \tag{7}$$

were also applied along the plate surface.

For each case, the total pressure and total temperature of the injected fluid was known, and the converging nozzle was presumed to be choked. Therefore, across the slot in the plane of the nozzle exit the following uniform conditions were applied:

$$p = p^* \tag{8}$$

$$T = T^* \tag{9}$$

$$u = 0 \tag{10}$$

$$v = v^* \tag{11}$$

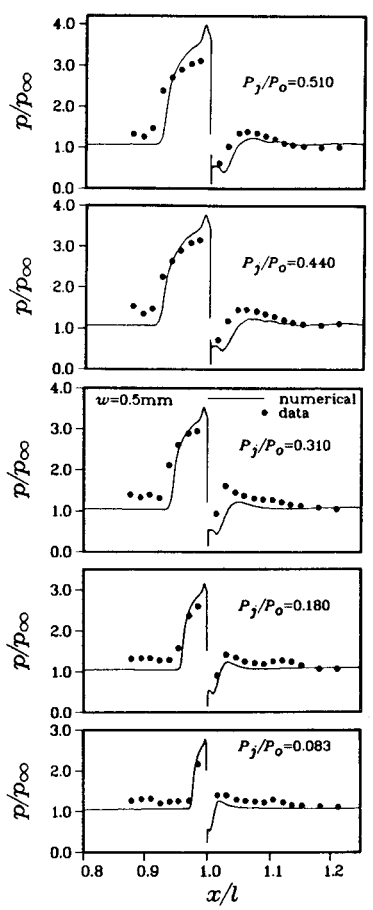


Fig. 5 Surface static pressure distributions for $w = 0.5$ mm.

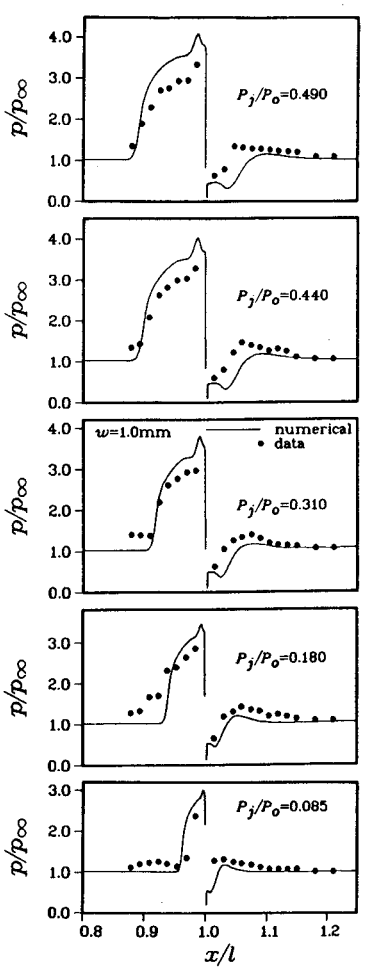


Fig. 6 Surface static pressure distributions for $w = 1.0$ mm.

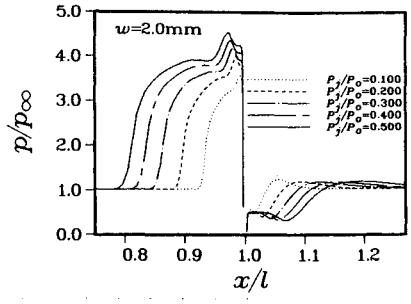


**Fig. 7 Surface static pressure distributions for $w = 2.0$ mm.**

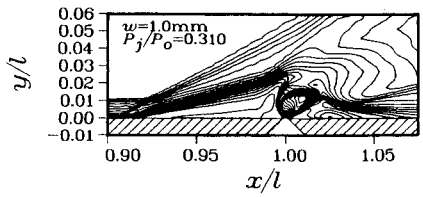


**Fig. 8 Mach number contours for $w = 1.0$ mm and $P_j/P_0 = 0.310$.**

together with

$$\frac{\partial k}{\partial n} = \frac{\partial \epsilon}{\partial n} = 0 \tag{12}$$

Because the flow is sonic at the plane of the nozzle exit, turbulence levels for $k$ and $\epsilon$ should be specified along this boundary. Such information, however, is not generally available for computational purposes and has been replaced by the simple conditions indicated by Eq. (12). Although the physical nozzle exit flow may not be precisely uniform, it is believed that this approximation closely resembles the experimental conditions[21] and is therefore deemed adequate for the numerical simulation.

## Numerical Procedure

The geometry consisted of a flat plate with a converging slot nozzle that is represented schematically in Fig. 1. The distance from the sharp leading edge to the centerline of the nozzle was prescribed as $l = 0.330$ m, corresponding to the experimental configuration. A nonuniform Cartesian computational mesh with its origin located at the leading edge of the flat plate was generated algebraically and consisted of $253 \times 81$ grid points in the $x$ and $y$ directions, respectively. The minimum $x$ mesh step size occurred across the nozzle exit where 32 uniformly spaced intervals were employed. Grid points in the streamwise direction were distributed away from the jet boundaries according to the one-dimensional stretching functions of Vinokur.[22] At the upstream and downstream ends of the domain, the mesh size was given by $\Delta x/l = 0.01$. Of the 253 $x$ grid points, 167 were located between the plate leading edge and the nozzle centerline.

In the normal direction, exponential stretching of $y$ grid lines was implemented from the plate surface to the upper boundary of the domain. Because the $k$-$\epsilon$ equations, particularly with the low Reynolds number terms, are sensitive to grid spacing at solid boundaries, $\Delta y$ was was chosen at the surface such that $y^+ < 1.0$ at the first $y$ mesh point above the plate for all solutions. It was found that this requirement was satisfied at all streamwise stations except in the immediate vicinity of the leading edge if $\Delta y/l = 0.00001$.

To examine the effect of grid resolution on the numerical solutions, computational grids consisting of $127 \times 41$ and $191 \times 61$ points were also generated. The coarse mesh $x$ grid point distribution was obtained from the fine grid by deleting every other $x$ grid line. All $y$ grid distributions were obtained by employing the same $\Delta y$ spacing at the wall and stretching to the outer boundary, thus maintaining the $y^+$ criterion. For clarity, only the coarse numerical grid ($127 \times 41$) is shown in Fig. 3 where the computational boundaries are evident.

Steady solutions to Eq. (1) were obtained using the time-dependent explicit unsplit two-step predictor-corrector finite difference algorithm of MacCormack,[23] which has proven to be a dependable technique for producing numerical solutions to a wide variety of complex fluid flow problems. Because of the explicit nature of this procedure, a time step-size limitation exists for stability. Although this limitation can be prohibitive, especially in view of the $y^+$ criterion for the present application, the overall reliability of the method and facility with which the $k$-$\epsilon$ equations could be implemented made the choice of this algorithm reasonable. As part of the procedure, a fourth-order pressure damping term,[24] commonly employed to suppress numerical oscillations arising from regions with large gradients in the dependent variables, was incorporated.

## Results

All of the results reported here were obtained via a fully vectorized computer code that was executed on a CRAY Y-MP 8/2128, achieving a mean data processing rate of $1.15 \times 10^{-5}$ CPU s/time step/grid point. A flat plate solution at the given flow conditions was generated on the coarse computational mesh and provided initial profiles to produce steady jet flow for $w = 1.0$ mm and $P_j/P_0 = 0.310$. This coarse jet solution was then interpolated to the fine grid and a converged steady result obtained. Initial conditions for all other jet cases were established on fine grids from previous steady solutions at either a different slot total pressure ratio or a different slot width. Computations were run at CFL numbers between 0.4 and 0.8 based on stability constraints and required 50,000–150,000 time steps per case to converge within plotting accuracy. However, to insure that no transients remained in the numerical flowfields, 100,000–350,000 total iterations were used to produce the final computed solutions.

The case corresponding to $w = 1.0$ mm and $P_j/P_0 = 0.310$ was selected for grid resolution study because it is representative of the injection experiments in terms of both slot width and slot total pressure ratio. Numerical solutions for this case were generated employing each of the aforementioned computational grids. Results of these calculations were compared in

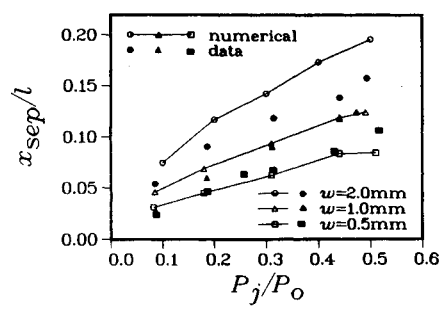


**Fig. 9 Separation length as function of slot total pressure ratio.**

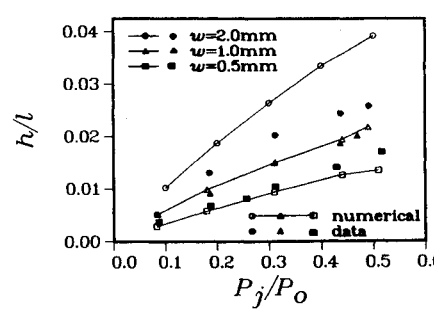


**Fig. 10 Height of the Mach surface as a function of slot total pressure ratio.**

terms of profiles at various streamwise locations, flowfield contours, and surface distributions of skin friction and static pressure. Because of the nature of the inviscid/viscous interacting flowfield, sensitivity with regard to the mesh distribution of shock waves as well as the size and shape of the recirculating flow regions were reflected in any of these comparisons. The surface static pressure distributions presented in Fig. 4 are thus typical of the variation in the solution with grid refinement. It is evident that on the finest mesh (253 × 81) the limit of grid convergence appears to have been approached. In all of the numerical results to follow, solutions will have been obtained on the finest computational mesh.

Computed surface static pressure distributions for a slot width $w = 0.5$ mm are compared with experimental data in Fig. 5. Agreement between the numerical results and the experiment is reasonable, particularly at lower values of the slot total pressure ratio. At higher values of $P_j/P_0$, the calculations overpredict the peak pressure level, underpredict the extent of the upstream interaction region, and overpredict the interaction length downstream. It should be noted that the experimental results do not indicate the sharp pressure peak just upstream of the slot leading edge that has been observed in the data of Spaid and Zukoski[7] and Werle et al.[8] and has been predicted numerically by Shang et al.[10] and by Thompson.[12] In addition, the measured pressure levels upstream of the interaction region are somewhat high due to leading-edge bluntness that evolved during the course of the experiment[21] but is unaccounted for numerically.

Figure 6 displays the corresponding surface pressure distributions for the slot width $w = 1.0$ mm. Here the comparison with experimental data is less favorable. Once again the computations overpredict the peak pressure level and generally overpredict the extent of the downstream interaction region. No experimental surface pressure data were reported for the case $w = 2.0$ mm, but for completeness numerical distributions are presented in Fig. 7. As expected, peak levels rise and the interaction region expands as the slot total pressure ratio increases.

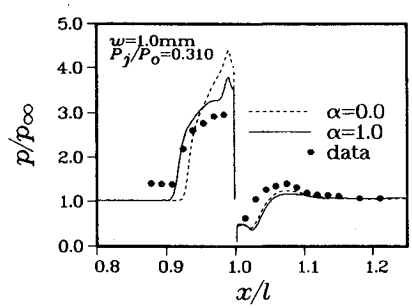


**Fig. 11 Effect of compressibility correction on surface static pressure distribution for $w = 1.0$ mm and $P_j/P_0 = 0.310$.**

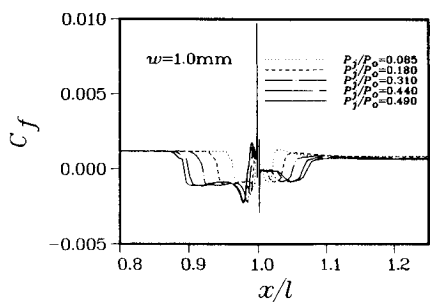


**Fig. 12 Skin friction coefficient distributions for $w = 1.0$ mm.**

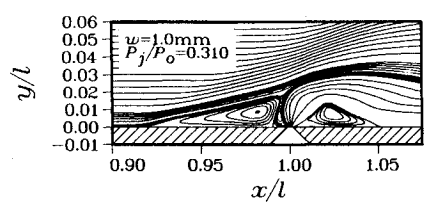


**Fig. 13 Stream function contours for $w = 1.0$ mm and $P_j/P_0 = 0.310$.**

Representative Mach number contours in the immediate vicinity of the nozzle exit for $w = 1.0$ mm and $P_j/P_0 = 0.310$ are shown in Fig. 8. The separation shock and Mach surface are quite visible, although these features are not clearly defined because of the diffusive nature of the MacCormack algorithm. Nevertheless, the figure may be used to infer the separation length $x_{sep}$ and the height of the Mach surface $h$. Here $x_{sep}$ is defined as the distance from the slot centerline to the point on the plate surface where the separation shock would intersect the wall if it extended undiminished through the boundary layer (see Fig. 2). This procedure is consistent with corresponding experimentally determined values that were deduced from schlieren photographs.

The nondimensional separation length is plotted as a function of slot total pressure ratio for all three slot widths and compared with experimental data in Fig. 9. Generally good agreement between the computations and the experiment is seen for $w = 0.5$ and 1.0 mm. For $w = 2.0$ mm, the numerical solutions overpredict the separation length by approximately 17%. Corresponding results for the nondimensional Mach surface height as a function of slot total pressure ratio appear in Fig. 10. Once again the agreement between the computations and the experimental data is good for $w = 0.5$ and 1.0 mm, but poor for $w = 2.0$ mm.

To assess the effect of the compressibility correction, the case $w = 1.0$ mm and $P_j/P_0 = 0.310$ was selected for investigation. By simply setting $\alpha = 0.0$, a numerical solution for this case was obtained without a dilatation dissipation term and compared with the prior result. Figure 11 displays the surface pressure distributions obtained from numerical solutions both with and without the compressibility correction, as well as with the experimental data. Inclusion of the correction is seen to reduce the peak pressure level upstream of the jet exit and to increase the extent of the upstream interaction region so that the numerically generated distribution more closely resembles that of the experiment. This dramatic change in the surface pressure indicates the sensitivity of the solution to turbulence parameters and evidences the difficulty of attempting to accurately simulate jet-injection flowfields.

Skin friction coefficient distributions for a slot width of $w = 1.0$ mm are presented in Fig. 12. Maximum and minimum wall shear levels are observed at the upstream and downstream edges of the jet nozzle. The length of the separated region is seen to grow linearly with increasing slot total pressure ratio, in correspondence with the results presented in Fig. 9.

Stream function contours for the same case are shown in Fig. 13 and indicate that the numerical solution has reproduced the commonly observed physical features of the jet interaction. The upstream clockwise rotating separated flow is clearly visible. Behind it is the narrow triangular region of counterclockwise recirculating fluid. This zone is bounded upstream by the dividing streamline, downstream by the forward jet streamline, and from below by the wall. Because the flow upstream of the dividing streamline is downward, and the jet flow is upward, the fluid in the triangular region is compelled to rotate in a counterclockwise direction. Near the top of this region, it can be observed that the flow coming from upstream must deflect upward abruptly to merge with the jet. This turning gives rise to the sharp peak in pressure upstream of the jet that was noted in Figs. 5–7. Downstream of the jet, the rearward clockwise recirculating region caused by the recompression shock is also evident.

## Conclusions and Discussion

Numerical solutions have been obtained for steady flowfields resulting from slot injection at the surface of a flat plate

in a freestream with a Mach number of 3.7 and a unit Reynolds number of $5.83 \times 10^6$/m. Effects of fine scale turbulence were represented by a two-equation ($k$-$\epsilon$) closure model that included a generalized formulation, low Reynolds number terms, and a compressibility correction. A grid mesh stepsize study indicated the adequacy of numerical resolution for the present application. Fifteen cases were considered, comprising a range of slot widths and slot total pressure ratios, and all distinctive features of the intricate flowfield structure appear to have been reproduced numerically.

Computed surface static pressure distributions compared reasonably well with experimental data for $w = 0.5$ mm, particularly at low total pressure ratios. A major disparity was noted in the peak pressure levels, which were higher numerically than the measurements. For the case $w = 1.0$ mm, pressure comparisons were less favorable. Agreement between the calculated separation length and Mach surface height and the corresponding experimental values was generally good for $w = 0.5$ and 1.0 mm, but poor for $w = 2.0$ mm. The primary cause for these disparities is attributed to three-dimensional effects in the experiment[21] that could not be simulated by the two-dimensional numerical calculations. In particular, because the wind-tunnel configuration has a finite span, spillage of the flow occurred over the spanwise edges of the model. This produced a relief effect, lowering the peak pressure level and decreasing the size of the recirculating flow regions. Predictably, the spillage increased with increasing slot width or slot total pressure ratio, producing additional relief consistent with numerical comparisons.

The effect of the compressibility correction by Sarkar et al.[15] was investigated. It was found that inclusion of a dilatation dissipation term in the turbulent kinetic energy equation reduced the magnitude of the peak pressure and increased the upstream extent of the interaction region in correspondence with experimental observations. Although the choice of the coefficient multiplying the correction term is somewhat arbitrary, no attempt was made to optimize its value.

## Acknowledgments

Computational resources for the work presented here were provided under the auspices of the Air Force Supercomputer Center, Eglin Air Force Base, Florida. The author is grateful to M. R. Visbal for helpful conversations, and to S. Aso for several useful discussions concerning details of the experiment.

## References

[1]Cubison, R. W., Anderson, B. H., and Ward, J. J., "Surface Pressure Distributions with a Sonic Jet Normal to Adjacent Flat Surfaces at Mach 2.92 and 6.4," NASA TN D-580, Feb. 1961.

[2]Zukoski, E. E., and Spaid, F. W., "Secondary Injection of Gases into a Supersonic Flow," *AIAA Journal,* Vol. 2, No. 10, 1964, pp. 1689–1696.

[3]Charwat, A. F., and Allegre, J., "Interaction of a Supersonic Stream and a Transverse Supersonic Jet," *AIAA Journal,* Vol. 2, No. 11, 1964, pp. 1965–1972.

[4]Schetz, J. A., and Billig, F. S., "Penetration of Gaseous Jets Injected into a Supersonic Stream," *Journal of Spacecraft and Rockets,* Vol. 3, No. 11, 1966, pp. 1658–1665.

[5]Hawk, N. E., and Amick, J. L., "Two-Dimensional Secondary Jet Interaction with a Supersonic Stream," *AIAA Journal,* Vol. 5, No. 4, 1967, pp. 655–660.

[6]Schetz, J. A., Hawkins, P. F., and Lehman, H., "Structure of Highly Underexpanded Transverse Jets in a Supersonic Stream," *AIAA Journal,* Vol. 5, No. 5, 1967, pp. 882–884.

[7]Spaid, F. W., and Zukoski, E. E., "A Study of the Interaction of Gaseous Jets from Transverse Slots with Supersonic External Flows," *AIAA Journal,* Vol. 6, No. 2, 1968, pp. 205–212.

[8]Werle, M. J., Driftmeyer, R. T., and Shaffer, D. G., "Jet-Interaction-Induced Separation: The Two-Dimensional Problem," *AIAA Journal,* Vol. 10, No. 2, 1972, pp. 183–193.

[9]Aso, S., Okuyama, S., Kawai, M., and Ando, Y., "Experimental Study on Mixing Phenomena in Supersonic Flows with Slot Injection," AIAA Paper 91-0016, Jan. 1991.

[10]Shang, J. S., McMaster, D. L., Scaggs, N., and Buck, M., "Interaction of Jet in Hypersonic Cross Stream," *AIAA Journal,* Vol. 27, No. 3, 1989, pp. 323–329.

[11]Rhie, C. M., and Syed, S. A., "Critical Evaluation of Three-Dimensional Supersonic Combustor Calculations," AIAA Paper 90-0207, Jan. 1990.

[12]Thompson, D. S., "Numerical Solution of a Two-Dimensional Jet in a Supersonic Crossflow Using an Upwind Relaxation Scheme," AIAA Paper 89-1869, June 1989.

[13]Lytle, J. K., Harloff, G. J., and Hsu, A. T., "Three-Dimensional Compressible Jet-in-Crossflow Calculations Using Improved Viscosity Models and Adapted Grid," AIAA Paper 90-2100, July 1990.

[14]Gerolymos, G. A., "Implicit Multiple-Grid Solutions of the Compressible Navier-Stokes Equations Using $k$-$\epsilon$ Turbulence Closure," *AIAA Journal,* Vol. 28, No. 10, 1990, pp. 1707–1717.

[15]Sarkar, S., Erlebacher, G., Hussaini, M. Y., and Kreiss, H. O., "The Analysis and Modeling of Dilatational Terms in Compressible Turbulence," NASA CR 181959, Dec. 1989.

[16]Jones, W. P., and Launder, B. E., "The Prediction of Laminarization with a Two-Equation Model of Turbulence," *International Journal of Heat and Mass Transfer,* Vol. 15, No. 2, 1972, pp. 301–314.

[17]Launder, B. E., and Sharma, B. I., "Application of the Energy-Dissipation Model of Turbulence to the Calculation of Flow Near a Spinning Disc," *Letters in Heat and Mass Transfer,* Vol. I, No. 2, 1974, pp. 131–138.

[18]Patel, V. C., Rodi, W., and Scheuerer, G., "Turbulence Models for Near-Wall and Low Reynolds Number Flows: A Review," *AIAA Journal,* Vol. 23, No. 9, 1985, pp. 1308–1319.

[19]Zeman, O., "Dilatation Dissipation: The Concept and Application in Modeling Compressible Mixing Layers," *Physics of Fluids A,* Vol. 2, No. 2, 1990, pp. 178–188.

[20]Rizzetta, D. P., "Numerical Simulation of Slot Injection into a Turbulent Supersonic Stream," AIAA Paper 92-0827, Jan. 1992.

[21]Aso, S., private communication, 1992.

[22]Vinokur, M., "One-Dimensional Stretching Functions for Finite-Difference Calculations," *Journal of Computational Physics,* Vol. 50, No. 2, 1983, pp. 215–234.

[23]MacCormack, R. W., "The Effect of Viscosity in Hypervelocity Impact Cratering," AIAA Paper 69-354, April 1969.

[24]MacCormack, R. W., and Baldwin, B. S., "A Numerical Method for Solving the Navier-Stokes Equations with Application to Shock-Boundary Layer Interaction," AIAA Paper 75-1, Jan. 1975.